American Mineralogist, Volume 93, pages 1470–1477, 2008

Unusual Al-Si ordering in calcic scapolite, $Me_{79.6}$, with increasing temperature

SYTLE M. ANTAO[1,*] AND ISHMAEL HASSAN[2]

[1]Advanced Photon Source, Argonne National Laboratory, Argonne, Illinois 60439, U.S.A.
[2]Department of Chemistry, University of the West Indies, Mona, Kingston 7, Jamaica

ABSTRACT

A scapolite sample, $Me_{79.6}$, from Slyudyanka, Siberia, Russia, has been studied using in situ synchrotron powder X-ray diffraction (XRD) and Rietveld structure refinements on heating from 26 to 900 °C and on cooling to about 300 °C. The structure was modeled and refined in space group *I4/m*. An accurate room-temperature structure was also obtained by using synchrotron high-resolution powder X-ray diffraction (HRPXRD) data and Rietveld structure refinement. From HRPXRD, the cell parameters are $a = 12.16711(2)$, $c = 7.575466(5)$ Å, and $V = 1121.461(3)$ Å^3; <T1-O> and <T2-O> are 1.643(1) and 1.672(1), respectively, so the T1 ($Al_{0.25}Si_{0.75}$) and T2 ($Al_{0.46}Si_{0.54}$) sites are partially ordered at room temperature. On heating, the <T-O> distances indicate that the T1 and T2 sites become more Si- and Al-rich, respectively, and therefore, ordering increases unusually with increasing temperature. This increase in Al-Si ordering occurs from 892 to 900 °C. At 900 °C, the T1 site becomes fully ordered with only Si atoms, while the T2 site contains $Al_{0.51}Si_{0.49}$ and therefore, is fully disordered. On cooling, the sample does not fully revert back to the original partially ordered state. At 300 °C, all the cell parameters are smaller because of the increased Al-Si ordering that is quenched in.

Keywords: Scapolite, high-temperature crystal structures, Al-Si ordering

INTRODUCTION

The scapolite series is a common group of rock-forming framework aluminosilicate minerals with formulae $(Na,Ca,K)_4[(Al,Si)_3Al_3Si_6O_{24}](Cl,CO_3,SO_4)$ that occur in a wide variety of metamorphic and altered igneous rocks (Deer et al. 1992). Scapolites may also be storage sites for volatiles in the lower crust and upper mantle (Lovering and White 1969), and may be an indicator of the activities of the volatile components (Jiang et al. 1994; Kullerud and Erambert 1999; Moecher and Essene 1990, 1991).

Scapolite forms solid solutions between the end-members marialite, $Na_4(Al_3Si_9O_{24})Cl = Me_0$, meionite, $Ca_4(Al_6Si_6O_{24})CO_3 = Me_{100}$, and $Ca_4(Al_6Si_6O_{24})SO_4$ (= silvialite = Me_{100}) (Deer et al. 1992; Teertstra et al. 1999). The meionite percentage [%Me = 100 Ca/(Na + Ca + K) = 25 Ca, as the M site is filled] may be used as a chemical index to indicate the compositions of scapolite (Shaw 1960). The scapolite composition varies by replacement of $(Na_4{\cdot}Cl)Si_2$ for $(NaCa_3{\cdot}CO_3)Al_2$ from Me_0-Me_{75} (series-1), whereas the meionite-rich end from Me_{75}-Me_{100} (series-2) is governed by the replacement of $(NaCa_3{\cdot}CO_3)Si$ for $(Ca_4{\cdot}CO_3)Al$ (Hassan and Buseck 1988). The cage clusters $(Na_4{\cdot}Cl)^{3+}$ and $(NaCa_3{\cdot}CO_3)^{5+}$ are ordered, whereas the clusters $(NaCa_3{\cdot}CO_3)^{5+}$ and $(Ca_4{\cdot}CO_3)^{6+}$ are disordered (Hassan and Buseck 1988). The $(Na_4{\cdot}Cl)^{3+}$ and $(NaCa_3{\cdot}CO_3)^{5+}$ clusters change from the ordered to the disordered state on heating (Antao and Hassan 2002); in particular, the Na-Ca atoms disorder with increasing temperature.

Seto et al. (2004) suggested that Me-rich scapolite is formed at high *T* with space group *I4/m* and, on rapid cooling, may not change to space group $P4_2/n$ and remained metastable at room *T*, thereby implying that an *I-P* transition exists for scapolite. High-*T* studies may reveal such a transition, if present.

Detailed in situ high-*T* structural data are not available for scapolite-group minerals. In addition to the importance of high-*T* structural characterization of the scapolite series, such data are important for determining the stability of scapolite, Al-Si ordering, Na-Ca ordering, and for understanding the antiphase domain boundaries (APBs) that are commonly observed, particularly, in intermediate scapolite.

High-*T* studies also have petrologic implications for thermodynamic and phase equilibria involving scapolite. For example, Moecher and Essene (1990) stated that Al-Si disorder in meionite has the greatest effect on derived phase relations. They also mentioned that available experimental data on meionite stability, XRD refinements, and nuclear magnetic resonance spectra for calcic scapolite do not uniquely constrain the Al-Si ordering state of synthetic meionite. However, the data are most consistent with a high degree of Al-Si disorder and inconsistent with long-range Al-Si order. Similar assumptions regarding Al-Si ordering were made by Goldsmith and Newton (1977) and Baker and Newton (1994). These assumptions need to be tested experimentally.

As a starting point for the high-*T* structural characterization of the scapolite series, a sample with composition $Me_{79.6}$ was chosen for this study because differential thermal analysis (DTA), thermogravimetry (TG), and differential scanning calorimetry (DSC) results for $Me_{79.6}$ showed no changes to 900 °C (Antao and Hassan 2002). These thermal analyses indicate that scapolite is stable until 1150 °C with loss of volatiles (CO_2 and NaCl) that occur around 1171 and 1232 °C. Therefore, $Me_{79.6}$ should be stable within the *T* range of the present study to 900 °C. However, this sample has minor inclusions of clusters from series-1 scapolite that are ordered in a homogeneous framework and may also contain antiphase domain boundaries (APBs) that arise from ordering of clusters (Hassan and Buseck 1988), or from Al-Si ordering (Seto et al. 2004).

* E-mail: sytle.antao@anl.gov

In this present study, we examined the structural evolution of $Me_{79.6}$ on heating from 26 to 900 °C and on cooling to about 300 °C (where the sample was lost). The Al and Si atoms are partially disordered in $Me_{79.6}$, so on heating, further disordering of atoms is generally expected. However, we observed the unusual behavior in which the T1 site becomes fully ordered with increasing T, and therefore, ordering increases unusually with increasing T (for the T1 site). This increasing Al-Si ordering occurs between 892 to 900 °C. On cooling, the sample does not fully revert back to the original partially disordered form within the time of the experiment.

Previous work

The framework of scapolite, $M_4(T_{12}O_{24})A$, $Z = 2$, consists of AlO_4 and SiO_4 tetrahedra, which form two types of four-membered rings. A Type-1 ring consists of T1 tetrahedra that point in the same direction, whereas Type-2 ring consists of T2 tetrahedra that point alternately up and down (Fig. 1). In space group $I4/m$, the T1 site has a multiplicity of 8 and that of T2 is 16. Five-membered rings occur along columns parallel to the **c** axis (Fig. 2). Continuous oval-shaped channels contain mainly Na^+ and Ca^{2+} cations with minor K^+ (=M site), and the large cages contain Cl^-, CO_3^{2-}, and SO_4^{2-} anions (=A site). Each A anion is coordinated by four M cations (Fig. 2). The resulting anion-cation cage clusters are centered at (0,0,0) and (½,½,½).

Several studies have been carried out on the scapolite series to examine trends in structural parameters (e.g., Sherriff et al. 2000, 1998; Sokolova et al. 1996, 2000; Teertstra et al. 1999; Teertstra and Sherriff 1996), and they divided the series into three subseries. Using TEM, the three subseries were confirmed, but the boundaries were modified by Seto et al. (2004). However, this division of the series into three is debatable, and will be addressed elsewhere. For the present purpose, we maintained the division of the series into two that meet at Me_{75} with series-1 from Me_0 to Me_{75} and series-2 from Me_{75} to Me_{100} (e.g., Evans et al. 1969; Hassan and Buseck 1988).

The a and V cell parameters of scapolite increase linearly during heating, whereas c remains essentially unchanged (Baker 1994; Graziani and Lucchesi 1982; Levien and Papike 1976). However, a decrease in the c parameter with increasing T was reported for marialite-rich scapolite (Kabalov et al. 1999). Although the unit-cell parameters were reversible on heating up to 800 °C (Baker 1994), permanent irreversible changes were observed on heating to 900 °C and cooling to room T (Levien and Papike 1976). The thermal expansion of scapolite is also a function of composition. The a and V increase approximately linearly with increasing %Me (Lin and Burley 1973), or with a trend inversely proportional to %Me (Graziani and Lucchesi 1982). However, Baker (1994) showed that this variation is nonlinear, especially for the Me-rich compositions. The cell parameters vary with framework composition and Al-Si order, but the influence of the interframework ions is only minor (Teertstra and Sherriff 1996).

Experimental methods

The scapolite sample, $Me_{79.6}$, is from a skarn deposit from Slyudyanka, Siberia, Russia. The crystals are white, bladed, and brittle (Evans et al. 1969). Crystals of scapolite were handpicked under a binocular microscope and finely ground in an agate mortar and pestle for the XRD experiments performed at the Advanced Photon Source, Argonne National Laboratory.

An accurate room-T structure was first obtained by using Rietveld structure refinement based on synchrotron high-resolution powder X-ray diffraction (HRPXRD) data from beam-line 11-BM. The sample was loaded into a kapton capillary and rotated during the experiment at a rate of 90 rotations/s. The data were collected to a maximum 2θ of about 50° with a step size of 0.0005° and a step time of 0.5 s/step. Beamline optics consists of a platinum-coated collimating mirror, a dual Si (111) monochromator, and a platinum-coated vertically focusing mirror. The HRPXRD traces were collected with twelve silicon crystal analyzers, which increase detector efficiency as well as reduce the angular range to be scanned, and therefore, allow rapid data acquisition. A silicon and alumina NIST standard (ratio of $1/3Si:2/3Al_2O_3$) was used to calibrate the detector response and

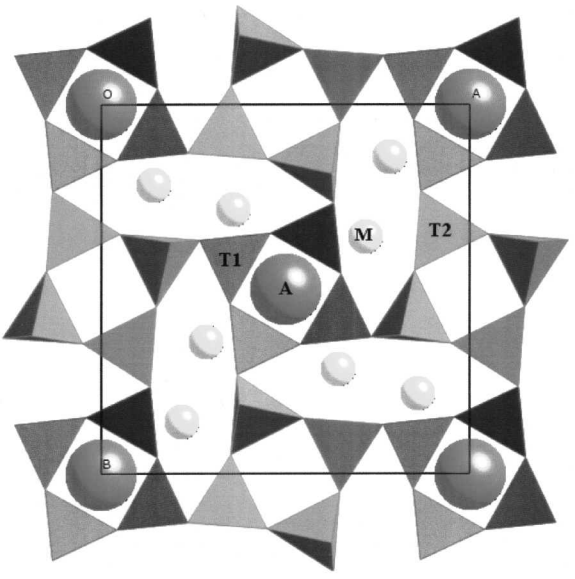

Figure 1. Structure of $I4/m$ scapolite projected along the **c** axis and showing the T, M, and A sites, as well as the four-membered rings and oval-shaped channels.

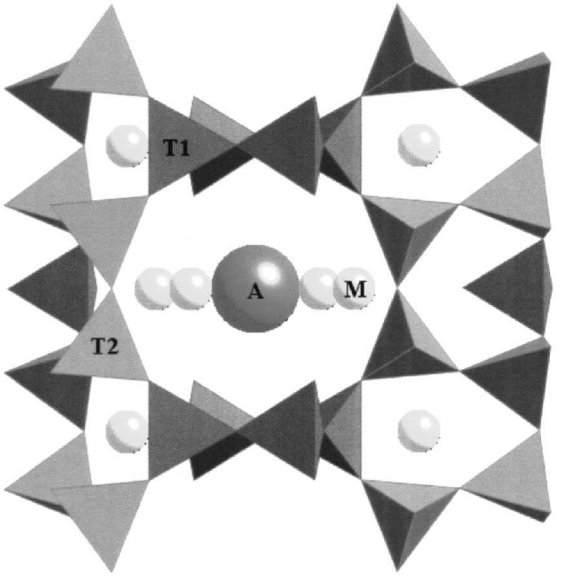

Figure 2. A part of $I4/m$ scapolite structure showing a cage containing the interstitial M cations and an A anion, and also a few five-membered rings.

zero offset, and to determine the wavelength used in the experiment [λ =0.60824(2) Å]. Data were merged by interpolating measured counts onto a regularly spaced grid and by applying corrections for small differences in wavelength (~1 eV). The HRPXRD trace is displayed in Figure 3.

The high-T synchrotron powder XRD experiments were performed at beamline 1-BM. The sample was loaded into a quartz capillary (diameter = 1 mm) and held in place by stuffing quartz wool at both ends of the open capillary. The capillary was oscillated during the experiment over a θ range of 2°. The in situ high-T XRD data were collected using synchrotron radiation [λ = 0.62260(5) Å] at room pressure and from about 26 to 900 °C. Elevated T were obtained using a heater and controlled using a thermocouple element placed inside the capillary and very close to the sample. The experimental error in T is about ±0.5 °C. Data were collected at a heating rate of about 7 °C/min. Data were also collected on air-cooling at a rapid rate of about 28 °C/min. The data were collected in regular intervals to a maximum 2θ of about 30°. An image plate (IP) detector (Mar345) mounted perpendicular to the beam path was used to collect full-circle Debye-Scherrer rings with an exposure time of 15 s. An external LaB_6 standard was used to determine the sample-to-detector distance, wavelength, and tilt of the IP. The diffraction patterns recorded by the IP were integrated using the Fit2d program to produce conventional I-2θ XRD traces (Hammersley et al. 1996). Examples of diffraction traces obtained at room and high T from the IP are displayed in Figure 4.

STRUCTURE REFINEMENTS

The chemical composition of $Me_{79.6}$ is $(Ca_{3.15}Na_{0.77}K_{0.04})(Si_{6.84}Al_{5.16}O_{24})Cl_{0.01}(CO_3)_{0.67}(SO_4)_{0.24}$ (Evans et al. 1969). Initial structural parameters were taken from the $Me_{72.2}$ silvialite structure of Teertstra et al. (1999). The XRD traces were modeled using the Rietveld method, as implemented in the GSAS program (Larson and Von Dreele 2000) and using the EXPGUI interface (Toby 2001). The structure refinement was carried out in the sequence of refining scale, background, cell, zero shift, profile, atomic positions, and displacement parameters. Finally, all variables were refined simultaneously. The HRPXRD data set at room T was refined first using anisotropic displacement parameters. We assumed that the M site is fully occupied by Na and Ca atoms and their occupancy factors were refined. We also assumed that the A site is fully occupied by only C and S atoms and their occupancy factors were refined. The occupancy factors for the O atoms belonging to the anion groups, O5S and O6C, were constrained to the occupancies of the C and S atoms and their isotropic displacement parameters were constrained to be equal to each other. This HRPXRD structural model was then

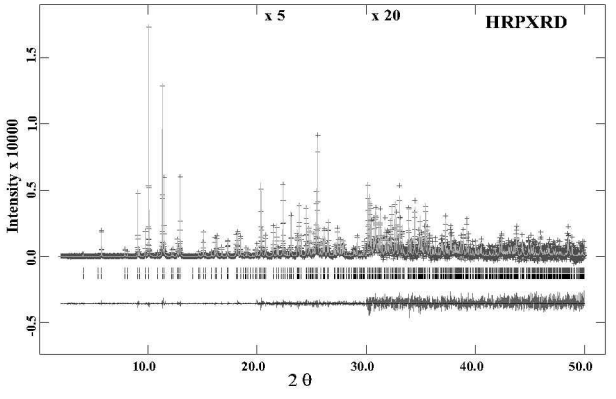

FIGURE 3. HRPXRD trace for scapolite, $Me_{79.6}$, at 25 °C, together with the calculated (continuous line) and observed (crosses) profiles. The difference curve ($I_{obs} - I_{calc}$) is shown at the bottom. The short vertical lines indicate allowed reflection positions. Note that the intensity beyond 20 and 30° is multiplied by 5 and 20, respectively, to improve clarity.

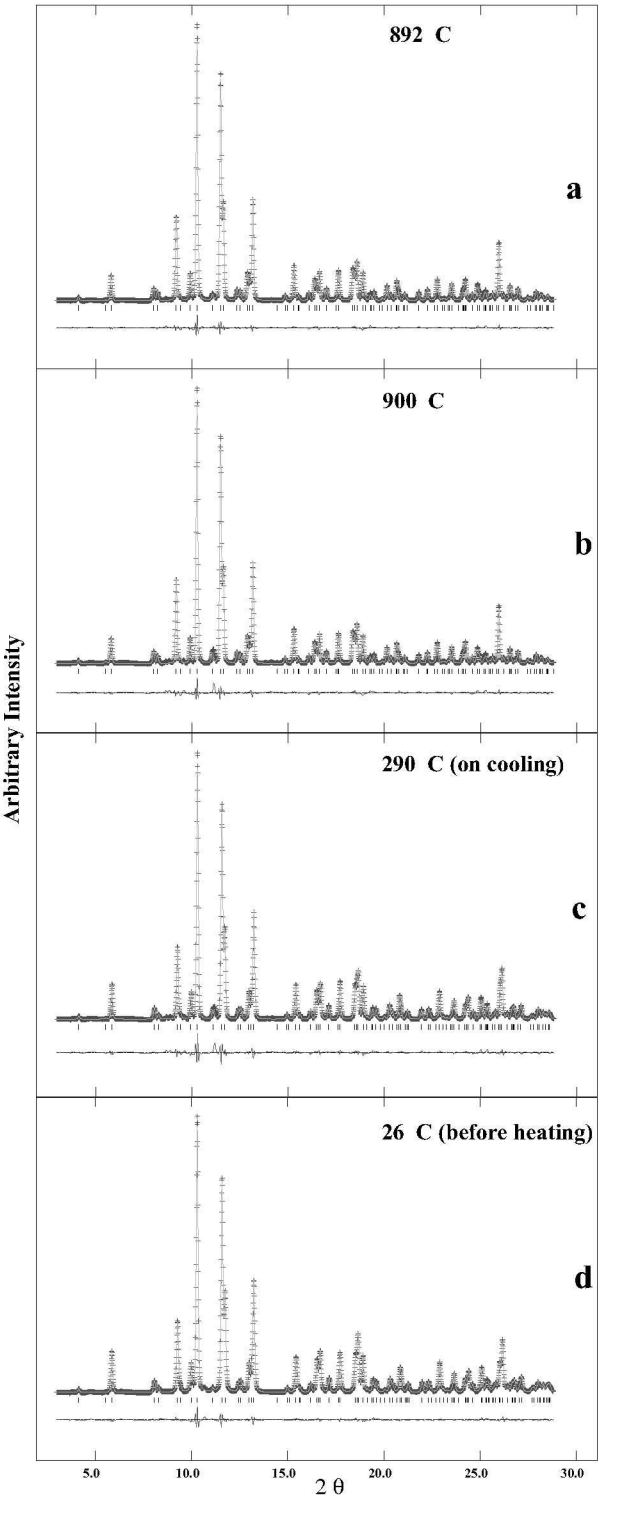

FIGURE 4. Comparison of the XRD traces for scapolite, $Me_{79.6}$, at (**a**) 892 °C, (**b**) 900 °C, (**c**) 290 °C on cooling, and (**d**) 26 °C before heating, together with the calculated (continuous line) and observed (crosses) profiles. The difference curve ($I_{obs} - I_{calc}$) is shown at the bottom. The short vertical lines indicate allowed reflection positions.

used for the image plate (IP) XRD data set at room T, which refined quite well and gave results similar to the HRPXRD structural parameters. The refined structural parameters were then used as input for the next higher-T structure. For all IP data, the occupancy factor for each site was held invariant and all the atoms were refined isotropically.

TABLE 1. Cell and Rietveld refinement statistics for scapolite at a few selected T

T (°C)	a (Å)	c (Å)	V (Å^3)	R_{F2}*
25 (HRPXRD)	12.16711(2)	7.575466(5)	1121.461(3)	0.0787
		Heating		
26	12.1667(2)	7.5758(2)	1121.44(3)	0.0238
101	12.1736(2)	7.5757(2)	1122.69(3)	0.0246
196	12.1834(2)	7.5761(2)	1124.55(3)	0.0250
296	12.1950(2)	7.5771(2)	1126.84(3)	0.0269
396	12.2067(2)	7.5780(2)	1129.16(3)	0.0275
494	12.2192(2)	7.5792(1)	1131.64(3)	0.0294
594	12.2322(2)	7.5806(1)	1134.27(3)	0.0311
694	12.2475(2)	7.5823(1)	1137.35(3)	0.0325
793	12.2618(2)	7.5841(1)	1140.27(3)	0.0355
900	12.2778(3)	7.5861(2)	1143.56(4)	0.0479
		Cooling		
894	12.2769(3)	7.5860(2)	1143.39(5)	0.0530
851	12.2707(3)	7.5853(2)	1142.11(5)	0.0551
793	12.2622(3)	7.5841(2)	1140.37(5)	0.0549
731	12.2532(3)	7.5829(2)	1138.49(5)	0.0541
665	12.2439(3)	7.5817(3)	1136.60(6)	0.0529
602	12.2354(3)	7.5805(3)	1134.82(6)	0.0505
540	12.2260(3)	7.5787(3)	1132.84(6)	0.0488
476	12.2172(3)	7.5772(3)	1130.97(6)	0.0470
413	12.2084(3)	7.5756(3)	1129.11(6)	0.0459
349	12.2008(3)	7.5746(3)	1127.55(6)	0.0441
290	12.1909(3)	7.5719(2)	1125.31(5)	0.0411

* R_{F2} = R-structure factor based on observed and calculated structure amplitudes = $[\sum(F_o^2 - F_c^2)^2/\sum(F_o^2)^2]^{1/2}$.

The cell parameters and refinement statistics are given in Table 1. The positional coordinates and displacement parameters are given in Table 2. Table 3 contains the anisotropic displacement parameters obtained from the HRPXRD data. Bond distances and angles are given in Table 4. All tables contain data for only a few selected T, but all the data are displayed graphically.

RESULTS AND DISCUSSION

The room-T structures obtained from the two different data sets are similar to each other, but obviously that obtained by HRPXRD is more accurate than the IP XRD data. However, the close similarity between the two structures at room T gives us confidence that detailed structural changes can be obtained at high T using our present IP XRD data.

The following cell parameters were obtained from the room-T HRPXRD data: a = 12.16711(2), c = 7.575466(5) Å, and V = 1121.461(3) Å^3. The average <T1-O> and <T2-O> distances are 1.643(1) and 1.672(1), respectively. These distances indicate that the site occupancies are ($Al_{0.25}Si_{0.75}$) for T1 and ($Al_{0.46}Si_{0.54}$) for T2, based on Si-O and Al-O distances of 1.6100(2) and 1.7435(2)

TABLE 3. Anisotropic displacement parameters (×100 Å^2) from HRPXRD data

Atom	U_{11}	U_{22}	U_{33}	U_{12}	U_{13}	U_{23}
T1	1.19(6)	1.29(7)	1.65(6)	0.21(5)	0	0
T2	1.75(5)	1.50(5)	1.42(4)	−0.20(4)	0.00(4)	−0.15(4)
M	1.72(6)	2.35(6)	4.07(8)	0.57(4)	0	0
A	0.56(23)	0.56(23)	0.87(28)	0	0	0
O1	1.91(15)	1.35(15)	2.15(16)	0.06(14)	0	0
O2	1.35(16)	1.85(16)	2.83(15)	0.49(11)	0	0
O3	3.99(12)	1.74(12)	2.19(12)	0.59(11)	0.64(10)	0.12(9)
O4	2.39(12)	2.02(11)	3.60(13)	0.28(10)	0.76(9)	0.42(9)

TABLE 2. Atomic positions and isotropic displacement parameters (× 100 Å^2) on heating at a few selected T

T (°C)		25 (HRPXRD)	26	101	196	296	396	494	594	694	793	900
T1	x	0.1604(1)	0.1621(3)	0.1621(3)	0.1622(3)	0.1623(3)	0.1623(3)	0.1624(3)	0.1626(3)	0.1628(3)	0.1629(3)	0.1608(4)
	y	0.0920(1)	0.0913(2)	0.0911(2)	0.0906(2)	0.0903(2)	0.0897(2)	0.0893(2)	0.0890(2)	0.0886(2)	0.0882(2)	0.0875(3)
	U	1.38*	1.6(1)	1.7(1)	1.9(1)	2.0(1)	2.1(1)	2.3(1)	2.3(1)	2.4(1)	2.5(1)	2.7(2)
T2	x	0.1603(1)	0.1592(2)	0.1593(2)	0.1593(2)	0.1594(2)	0.1593(2)	0.1594(2)	0.1594(2)	0.1592(2)	0.1591(2)	0.1580(3)
	y	0.4131(1)	0.4132(2)	0.4134(2)	0.4136(2)	0.4139(2)	0.4142(2)	0.4146(2)	0.4151(2)	0.4156(2)	0.4161(2)	0.4171(2)
	z	0.2068(1)	0.2070(3)	0.2071(3)	0.2070(3)	0.2070(3)	0.2071(3)	0.2070(3)	0.2069(3)	0.2067(3)	0.2065(3)	0.2055(3)
	U	1.55*	1.24(7)	1.32(7)	1.42(7)	1.50(7)	1.62(7)	1.74(7)	1.91(8)	2.01(8)	2.12(8)	2.7(1)
M	x	0.3582(1)	0.3580(2)	0.3579(2)	0.3579(2)	0.3579(2)	0.3578(2)	0.3578(2)	0.3578(2)	0.3578(2)	0.3580(2)	0.3556(3)
	y	0.2830(1)	0.2843(2)	0.2844(2)	0.2845(2)	0.2847(2)	0.2849(2)	0.2851(2)	0.2850(2)	0.2852(2)	0.2852(2)	0.2858(3)
	U	2.71*	2.95(9)	3.3(1)	3.6(1)	4.0(1)	4.3(1)	4.8(1)	5.1(1)	5.6(1)	6.0(1)	6.1(2)
A	U	0.67*	1.3(4)	1.6(4)	2.0(5)	2.3(5)	2.4(5)	2.7(5)	3.5(5)	3.5(5)	4.0(5)	5.2(8)
O1	x	0.0411(2)	0.0405(4)	0.0406(4)	0.0406(4)	0.0408(4)	0.0408(4)	0.0411(4)	0.0412(4)	0.0413(4)	0.0414(5)	0.0436(6)
	y	0.1505(2)	0.1492(4)	0.1488(4)	0.1486(4)	0.1481(4)	0.1479(4)	0.1474(4)	0.1470(4)	0.1462(4)	0.1456(4)	0.1478(5)
	U	1.80*	1.5(2)	1.6(2)	1.9(2)	2.2(2)	2.4(2)	2.8(2)	3.3(2)	3.6(2)	4.0(3)	3.5(3)
O2	x	0.1857(2)	0.1855(4)	0.1856(4)	0.1856(4)	0.1856(4)	0.18570(41)	0.1857(4)	0.1857(4)	0.1859(5)	0.1859(5)	0.1896(5)
	y	0.3743(2)	0.3749(3)	0.3755(3)	0.3764(3)	0.3772(3)	0.37799(28)	0.3788(3)	0.3796(3)	0.3806(3)	0.3814(3)	0.3804(4)
	U	2.01*	2.1(2)	2.4(2)	2.6(2)	3.0(2)	3.2(2)	3.7(2)	4.0(2)	4.2(2)	4.5(2)	3.9(3)
O3	x	0.4502(1)	0.4507(3)	0.4508(4)	0.4506(3)	0.4506(3)	0.45053(34)	0.4505(3)	0.4501(4)	0.4500(4)	0.4497(4)	0.4492(5)
	y	0.1496(1)	0.1507(3)	0.1504(3)	0.1503(3)	0.1501(3)	0.14988(28)	0.1497(3)	0.1497(3)	0.1494(3)	0.1492(3)	0.1482(4)
	z	0.2068(2)	0.2078(4)	0.2083(4)	0.2089(4)	0.2095(4)	0.2102(4)	0.2108(4)	0.2117(5)	0.2128(5)	0.2139(5)	0.2186(6)
	U	2.64*	2.9(2)	3.1(2)	3.5(2)	3.8(2)	4.1(2)	4.6(2)	4.9(2)	5.3(2)	5.6(2)	5.1(2)
O4	x	0.2664(1)	0.2660(2)	0.2661(2)	0.2662(2)	0.2663(2)	0.26645(23)	0.2665(2)	0.2663(3)	0.2664(3)	0.2662(3)	0.2658(3)
	y	0.3665(1)	0.3670(2)	0.3674(2)	0.3681(2)	0.3686(2)	0.36926(20)	0.3699(2)	0.3707(2)	0.3714(2)	0.3721(2)	0.3731(3)
	z	0.6735(2)	0.6717(5)	0.6713(5)	0.6711(5)	0.6706(5)	0.6703(5)	0.6702(5)	0.6702(5)	0.6698(5)	0.6697(5)	0.6619(7)
	U	2.67*	2.7(2)	2.7(2)	2.9(2)	3.0(2)	3.2(2)	3.4(2)	3.7(2)	3.9(2)	4.1(2)	5.3(2)
O5S	x	0.3930(26)	0.3836(55)	0.3791(53)	0.3761(51)	0.3730(49)	0.3705(48)	0.3703(48)	0.3712(50)	0.3687(50)	0.3700(53)	0.4143(56)
	y	0.4893(42)	0.5736(61)	0.5738(59)	0.5769(57)	0.5782(56)	0.5809(56)	0.5784(56)	0.5779(59)	0.5775(59)	0.5785(64)	0.5020(80)
	z	0.1276(45)	0.1047(73)	0.1065(74)	0.1082(74)	0.1081(75)	0.1078(76)	0.1103(80)	0.1092(83)	0.1102(87)	0.1081(92)	0.2041(99)
	U	10.80(27)	9.2(5)	9.5(5)	9.9(5)	10.3(5)	10.9(5)	11.8(6)	12.2(6)	12.7(6)	13.7(6)	18.2(11)
O6C	x	0.6010(5)	0.6006(7)	0.6003(7)	0.5998(7)	0.5996(7)	0.5991(7)	0.5992(7)	0.5986(7)	0.5982(8)	0.5976(8)	0.6026(12)
	y	0.5142(8)	0.5113(17)	0.5113(17)	0.5109(17)	0.5100(16)	0.5100(17)	0.5092(17)	0.5089(17)	0.5083(18)	0.5076(19)	0.4982(26)

Notes: T1, O1, O2, O6C, and M are at (x,y,0); A is at (½,½,0). Site occupancies from HRPXRD data are as follows: Si was placed in T1 and T2 sites and occupancies determined from T-O distances; the M site contains 0.794(5) Ca and 0.206(5) Na; and A site contains 0.834(7) C and 0.146(7) S, whereas O5S was 0.073(4) and O6C was 0.625(5). O1 to O4 sites were fully occupied. A short distance, O5S-O6C = 0.97(4) Å, arises from disorder of the anion groups.

* For HRPXRD data, U_{eq} are given, except for U(O5S) = U(O6C) that was refined isotropically.

TABLE 4. Selected interatomic distances (Å) and angles (°) on heating at a few selected T

T (°C)	25 (HRPXRD)	26	101	196	296	396	494	594	694	793	900
T1-O1	1.618(2)	1.639(5)	1.638(5)	1.641(5)	1.641(5)	1.644(5)	1.644(5)	1.646(5)	1.647(5)	1.647(5)	1.618(7)
T1-O1′	1.623(2)	1.611(4)	1.610(4)	1.607(4)	1.608(4)	1.603(4)	1.603(4)	1.604(5)	1.604(5)	1.603(5)	1.618(6)
T1-O4 ×2	1.666(2)	1.648(4)	1.645(4)	1.642(4)	1.637(4)	1.635(4)	1.634(4)	1.633(4)	1.628(4)	1.628(4)	1.599(5)
<T1-O>	1.643(1)	1.637(2)	1.635(2)	1.633(2)	1.631(2)	1.629(2)	1.629(2)	1.629(2)	1.627(2)	1.627(2)	1.609(3)
T2-O2	1.665(1)	1.667(2)	1.666(2)	1.664(2)	1.662(2)	1.662(2)	1.660(2)	1.659(2)	1.658(2)	1.656(2)	1.669(3)
T2-O3	1.669(2)	1.658(4)	1.657(4)	1.658(4)	1.657(4)	1.655(4)	1.653(4)	1.653(4)	1.650(4)	1.651(4)	1.649(5)
T2-O3′	1.679(1)	1.677(3)	1.677(3)	1.675(3)	1.675(3)	1.674(3)	1.676(3)	1.674(3)	1.673(4)	1.669(4)	1.645(5)
T2-O4	1.677(2)	1.687(3)	1.688(3)	1.690(3)	1.693(3)	1.695(3)	1.695(3)	1.695(3)	1.701(3)	1.701(3)	1.749(4)
<T2-O>	1.672(1)	1.672(2)	1.672(2)	1.672(2)	1.672(2)	1.672(2)	1.671(2)	1.670(2)	1.670(2)	1.669(2)	1.678(2)
M-O2	2.375(2)	2.371(5)	2.373(5)	2.379(5)	2.384(5)	2.389(5)	2.394(5)	2.402(5)	2.408(5)	2.417(5)	2.345(6)
M-O3 ×2	2.518(2)	2.529(4)	2.536(4)	2.541(4)	2.548(4)	2.556(4)	2.564(4)	2.568(4)	2.577(4)	2.585(4)	2.631(5)
M-O4 ×2	2.898(2)	2.907(4)	2.910(4)	2.914(4)	2.920(4)	2.923(4)	2.927(4)	2.932(4)	2.939(4)	2.945(4)	2.990(5)
M-O4′ ×2	2.708(2)	2.712(3)	2.716(3)	2.725(3)	2.731(3)	2.740(3)	2.749(3)	2.756(3)	2.765(3)	2.774(3)	2.745(4)
<M-O>[7]	2.660(1)	2.667(1)	2.671(1)	2.677(1)	2.683(1)	2.690(1)	2.696(1)	2.702(1)	2.710(1)	2.718(1)	2.725(2)
M-O6C	2.517(10)	2.538(20)	2.539(20)	2.545(20)	2.557(19)	2.558(20)	2.568(20)	2.576(21)	2.587(21)	2.598(23)	2.702(31)
M-O6C′	2.366(8)	2.333(19)	2.335(19)	2.336(18)	2.331(18)	2.336(18)	2.329(19)	2.333(19)	2.331(20)	2.331(21)	2.223(25)
<M-O>[9]	2.612(2)	2.615(3)	2.619(3)	2.624(3)	2.630(3)	2.636(3)	2.641(3)	2.647(3)	2.654(3)	2.662(4)	2.667(5)
M-A	3.154(1)	3.143(2)	3.143(2)	3.145(2)	3.146(2)	3.148(2)	3.149(2)	3.153(2)	3.155(3)	3.157(3)	3.172(4)
S-O5S ×8	1.63(3)	1.85(5)	1.90(5)	1.96(5)	1.99(5)	2.04(5)	2.03(5)	2.02(5)	2.05(5)	2.03(5)	1.87(10)
C-O6C ×4	1.241(7)	1.232(8)	1.229(8)	1.223(8)	1.221(8)	1.216(8)	1.218(8)	1.211(9)	1.207(9)	1.200(9)	1.260(14)
T1-O1-T1	158.1(2)	160.2(4)	160.4(4)	160.4(4)	160.7(4)	160.7(4)	160.9(4)	161.3(4)	162.0(4)	162.3(4)	158.4(6)
T2-O2-T2	140.5(1)	140.4(3)	140.7(3)	141.0(3)	141.3(3)	141.6(3)	141.9(3)	141.9(3)	142.0(3)	142.2(3)	138.2(3)
T2-O3-T2	146.5(1)	145.8(3)	146.2(3)	146.3(3)	146.6(3)	146.8(3)	147.1(3)	147.1(3)	147.4(3)	147.6(3)	148.5(4)
T1-O4-T2	137.4(1)	137.4(2)	137.6(2)	137.8(2)	137.9(2)	138.1(2)	138.3(2)	138.5(2)	138.7(2)	138.9(2)	140.8(3)
<T-O-T>	145.6(1)	145.9(1)	146.2(1)	146.4(1)	146.6(1)	146.8(1)	147.0(1)	147.2(1)	147.5(1)	147.8(2)	146.5(2)

Å, respectively, as was observed in sodalite, $Na_8(Al_6Si_6O_{24})Cl_2$ (our unpublished data). Therefore, the T1 and T2 sites are partially ordered at room T. The anion groups are disordered. Our structure is similar to the $Me_{72.2}$ structure (Teertstra et al. 1999), and the Me_{93} structure for the sample from Monte Somma, Italy (e.g., Lin and Burley 1973; Ulbrich 1973). Our refined site occupancy factors are similar to those obtained from the chemical analysis. In particular, the refined occupancy factor for the Ca site is 0.794(5) and gives rise to $Me_{79.4}$ compared to $Me_{79.6}$ obtained from chemical analysis.

The variations of cell parameters for $Me_{79.6}$ with T are shown in Figure 5. At room T, our cell parameters match quite closely with the data from HRPXRD. On heating to 900 °C, all cell parameters increase smoothly but nonlinearly. On cooling from 900 to 290 °C, the cell parameters revert on a different path, especially the c cell parameter (Fig. 5b). When the cell parameters are plotted as d/d_0 ratio, it can be seen that the **a** axis expands much more than the **c** axis (Fig. 6). These results contrast with previous studies where linear increases were reported for a and V, but c was nearly constant (Baker 1994; Graziani and Lucchesi 1982; Levien and Papike 1976). A decrease in c with T was reported by Kabalov et al. (1999).

The variations of selected bond distances and bridging angles with T are given (Figs. 7 and 8). The average <T1-O> and <T2-O> distances show a slight decrease with T mainly because of thermal motion; however, between 892 and 900 °C, these distances change considerably. At 892 °C, the <T1-O> and <T2-O> distances are 1.624(2) and 1.670(8) Å, respectively, whereas at 900 °C, the <T1-O> and <T2-O> distances are 1.609(3) and 1.678(2) Å, respectively. Therefore, the changes from 892 and 900 °C are –0.92 and +0.46% for the <T1-O> and <T2-O> distances, respectively. The T1 and T2 are on eightfold and sixteenfold sites, respectively. These changes can be compared to –1.74 and 0.37% between 26 and 900 °C for the corresponding T1 and T2 sites (Fig. 7a). From 892 and 900 °C, the T2 site becomes more Al rich (T2 from $Al_{0.45}Si_{0.55}$ to $Al_{0.51}Si_{0.49}$), while the T1 site becomes more Si rich (T1 from $Al_{0.1}Si_{0.9}$ to $Al_{0.0}Si_{1.0}$; i.e., full ordering of T1 occurs at 900 °C). Therefore, in scapolite $Me_{79.6}$, Al-Si ordering increases with T to the maximum extent allowed for the T1 site at 900 °C. This is quite an unusual behavior as we generally expect atoms to disorder with increasing T. On cooling, the Al-Si ordering does not revert back to the original disordered form. All the bridging angles change slightly with T and sharp changes (increases/decreases) are observed near 900 °C (Figs. 7b and 7c). Small amounts of Al-Si order and changes in cell parameters (before and after heating) were also reported for an intermediate scapolite by Levien and Papike (1976).

The present study shows significant Al-Si ordering at all T. Consequently, the assumptions regarding Al-Si disorder and its implications for thermodynamic and phase equilibria involving scapolite may not be valid. For example, Moecher and Essene (1990) stated that their data are most consistent with a high degree of Al-Si disorder and inconsistent with long-range Al-Si order. Similar assumptions were made by Goldsmith and Newton (1977) and Baker and Newton (1994).

The <M-O> distances increase significantly with T and are responsible for the expansion of the scapolite structure (Fig. 8a). The expansion of the <M-O> distances gives rise to rotations of the TO_4 tetrahedra, which are indicated by changes in the bridging T-O-T angles. Except for T1-O4-T2 angle, the other T-O-T angles are nearly unchanged until about 900 °C (Fig. 7c). Therefore, the expansion of the <M-O> distances is mainly responsible for the expansion of the scapolite structure, in contrast to TO_4 rotation proposed by Levien and Papike (1976). However, as a result of <M-O> expansion, TO_4 tetrahedral rotations do occur and are discussed further below. The variation of the M-A distance is

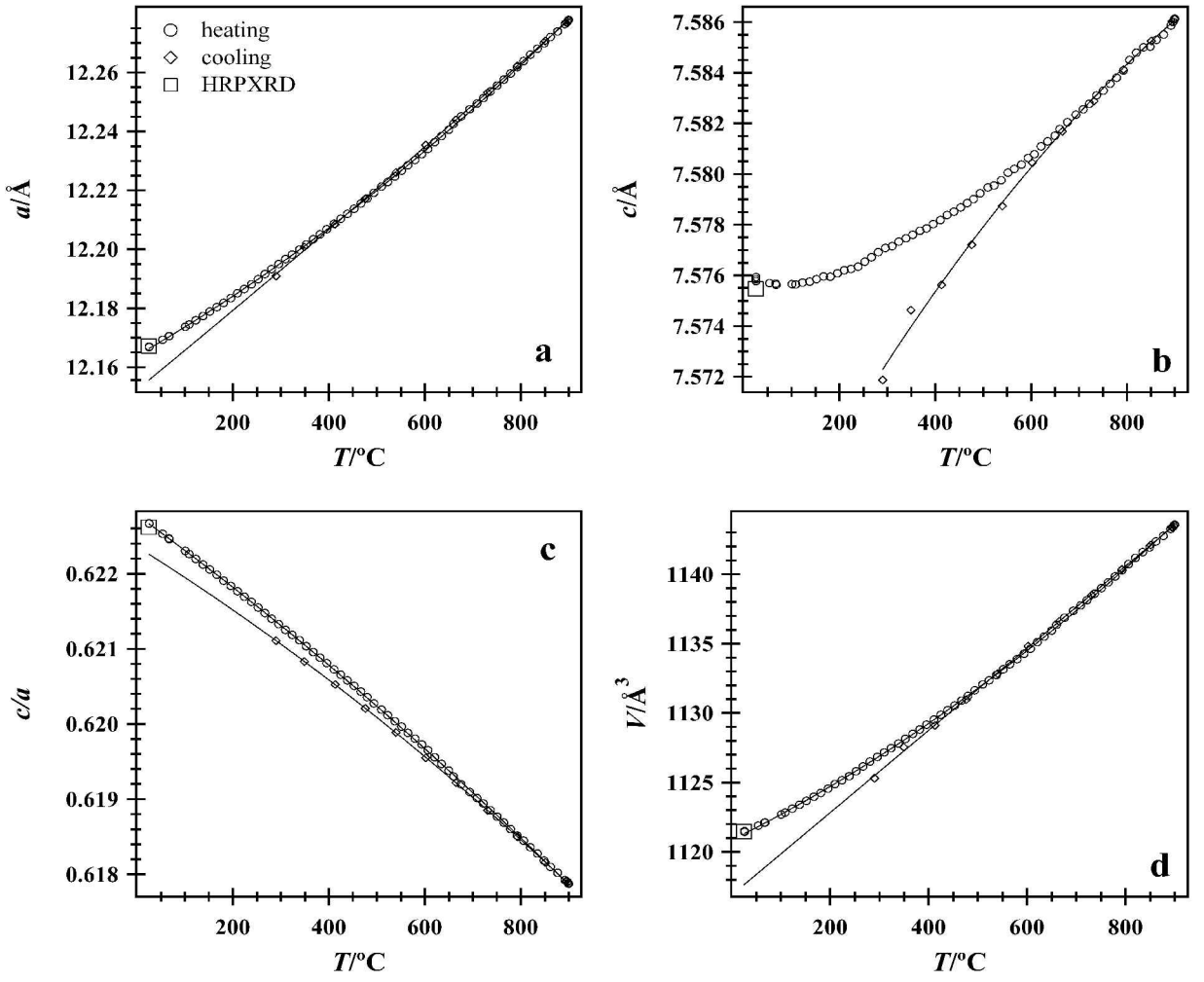

FIGURE 5. Variation of unit-cell parameters with T. (**a**) a, (**b**) c, (**c**) c/a ratio, and (**d**) V. In this and all graphs below, error bars are smaller than the symbols, if they are not seen. Solid lines are polynomial fits that are used as guides to the eye. In this and the following graphs, the few data points on cooling are displayed and the large symbols at room T are from the HRPXRD data.

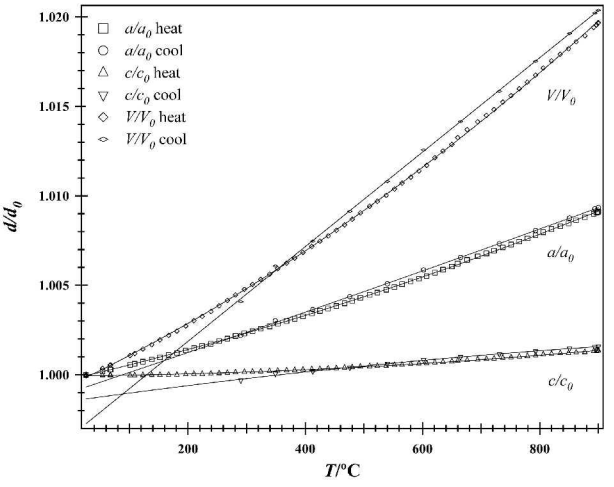

FIGURE 6. Axial and volume unit-cell parameters plotted with d/d_0 as a function of T. The c/c_0 increases slightly, while the a/a_0 expansion is high.

shown in Figure 8b.

The variations of the S-O5S and C-O6C distances with T are shown (Fig. 8c). These rigid anion groups are not expected to vary with T, but their positional disorder and the small amount of electron density, especially for the O5S atom, indicate that they may not be modeled properly.

The displacement parameters vary smoothly with T (Figs. 9a and 9b). The T sites have the smallest displacement parameters followed by increasing values for framework O atoms, M cations, A site, then O5S/O6C. Large displacement parameters occur for the anion groups because they are disordered. As the M cations are also bonded to the anion groups, they may also be affected by the disorder of the anion groups, and possible cluster ordering complicates the matter further.

In Figure 10, the oval channels are displayed at room T. The long and short diameters are 9.393 and 3.106 Å, respectively, at room T (from HRPXRD data) and 9.360 and 3.327 Å, respectively, at 900 °C. Therefore, with increasing T, the oval channels open up as the short diameter increases (Fig. 11), as indicated by Levien and Papike (1976). However, the main reason for the

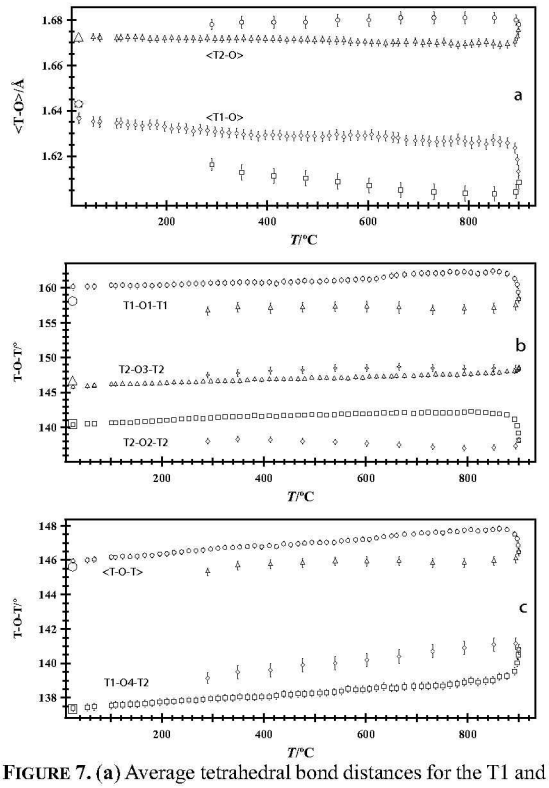

FIGURE 7. (**a**) Average tetrahedral bond distances for the T1 and T2 sites; tetrahedral bridging angles as a function of T (**b**, **c**).

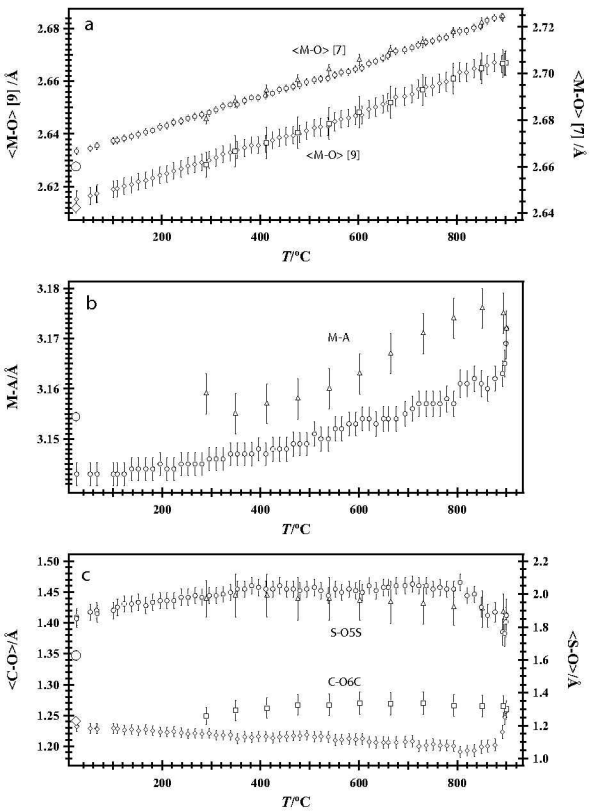

FIGURE 8. (**a**) Average <M-O>, (**b**) M-A, and (**c**) C-O6C and S-O5S distances as a function of T.

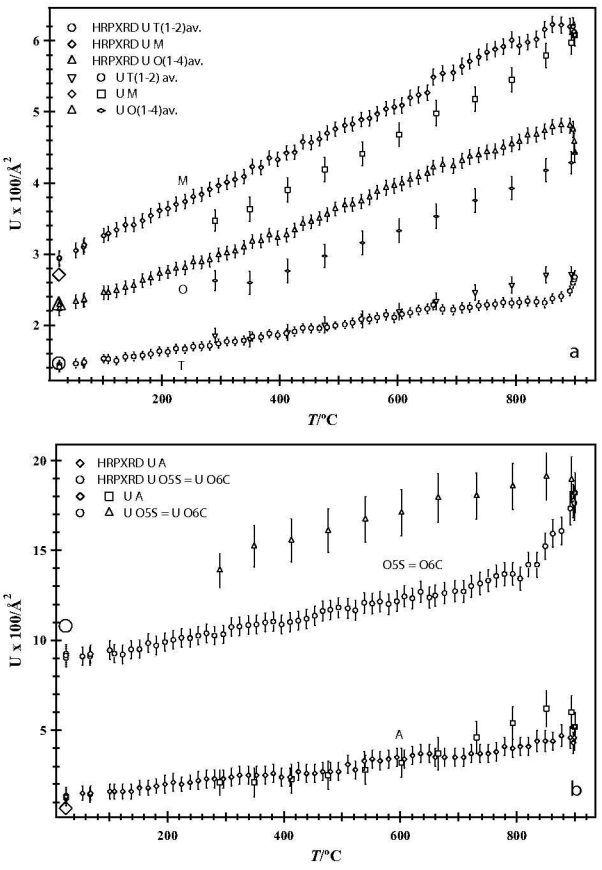

FIGURE 9. Variation of isotropic displacement parameters, U, as a function of T (**a**, **b**). The values of these parameters decrease in the following order: T < O(1-4) < M < A << O(S/C).

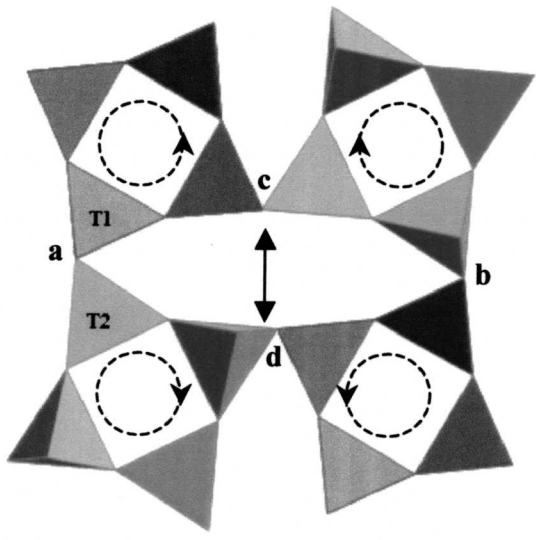

FIGURE 10. Double-headed arrows indicate opening of the oval-shaped channels that arise from rotation of the TO_4 tetrahedra "out" as indicated by the arrows in the four-membered rings. These openings and rotations are caused by expansion of the <M-O> and M-A distances and gives rise to a more-open framework structure.

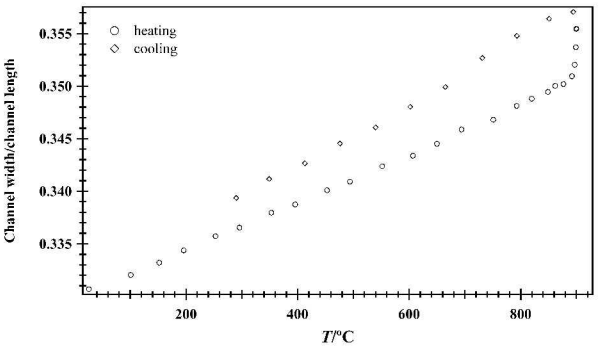

FIGURE 11. Variation of the channel-width ratio (short axis O4a-O4b/long axis O4c-O4d) with increasing T. The increase is linear to 877 °C, and higher increases occur from 892 to 900 °C.

expansion of the scapolite structure arises from the expansion of the <M-O> and M-A distances that causes the TO_4 tetrahedra to rotate "out" and gives rise to opening of the oval-shaped channels, resulting in a more open framework structure (Figs. 10 and 11).

Seto et al. (2004) suggested that Me-rich scapolite may have an *I-P* transition, which was not observed in this study. Clustering occurs in series-1 scapolite, and they are disordered on heating at about 300 °C (Antao and Hassan 2002; Hassan and Buseck 1988), while Al-Si ordering changes at about 900 °C (this study).

Scapolite $Me_{79.6}$ contains partially ordered Al-Si atoms in the T1 and T2 sites at room T. With increasing T, all the cell parameters increase smoothly but nonlinearly. On cooling, all the cell parameters change because of the unusual change of increasing Al-Si ordering that is quenched in. On heating to 900 °C, the T1 site becomes fully ordered. The change in Al-Si ordering that is quenched in gives rise to smaller values for all the cell parameters on cooling. Increasing T causes the <M-O> and <M-A> distances to increase and forces the TO_4 tetrahedra to rotate "out" and create a more open structure by expansion of the short diameters of the oval-shaped channels.

ACKNOWLEDGMENTS

We thank the two anonymous reviewers and the editor, L. Galoisy, for providing useful comments. P.L. Lee is thanked for his help with the 1-BM experiment. We thank D.M. Shaw for providing the scapolite sample. XRD data were collected at the X-ray Operations and Research beamline 1-BM and 11-BM at the Advanced Photon Source, Argonne National Laboratory. Use of the Advanced Photon Source was supported by the U.S. Department of Energy, Office of Science, Office of Basic Energy Sciences, under contract no. DE-AC02-06CH11357.

REFERENCES CITED

Antao, S.M. and Hassan, I. (2002) Thermal behavior of scapolite $Me_{79.6}$ and $Me_{33.3}$. Canadian Mineralogist, 40, 1395–1401.

Baker, J. (1994) Thermal expansion of scapolite. American Mineralogist, 79, 878–884.

Baker, J. and Newton, R.C. (1994) Standard thermodynamic properties of meionite, $Ca_4Al_6Si_6O_{24}CO_3$, from experimental phase-equilibrium data. American Mineralogist, 79, 478–484.

Deer, W.A., Howie, R.A., and Zussman, J. (1992) An Introduction to the Rock-forming Minerals, 2nd edition. John Wiley, New York.

Evans, B.W., Shaw, D.M., and Haughton, D.R. (1969) Scapolite stoichiometry. Contributions to Mineralogy and Petrology, 24, 293–305.

Goldsmith, J.R. and Newton, R.C. (1977) Scapolite-plagioclase stability relations at high pressures and temperatures in the system $NaAlSi_3O_8$-$CaAl_2Si_2O_8$-$CaCO_3$-$CaSO_4$. American Mineralogist, 62, 1063–1081.

Graziani, G. and Lucchesi, S. (1982) The thermal behavior of scapolites. American Mineralogist, 67, 1229–1241.

Hammersley, A.P., Svensson, S.O., Hanfland, M., Fitch, A.N., and Hausermann, D. (1996) Two-dimensional detector software: from real detector to idealised image to two-theta scan. High Pressure Research, 14, 235–248.

Hassan, I. and Buseck, P.R. (1988) HRTEM characterization of scapolite solid solutions. American Mineralogist, 73, 119–134.

Jiang, S.Y., Palmer, M.R., Xue, C.J., and Li, Y.H. (1994) Halogen-rich scapolite-biotite rocks from the Tongmugou Pb-Zn deposit, Qinling, north-western China: Implications for the ore-forming process. Mineralogical Magazine, 58, 543–552.

Kabalov, Y.K., Sokolova, E.V., Kalygina, N.V., and Schneider, J. (1999) Changes in the crystal structure of marialite during heating. Crystallography Reports, 44, 979–983.

Kullerud, K. and Erambert, M. (1999) Cl-scapolite, Cl-amphibole, and plagioclase equilibria in ductile shear zones at Nusfjord, Lofoten, Norway: Implications for fluid compositional evolution during fluid-mineral interaction in the deep crust. Geochimica et Cosmochimica Acta, 63, 3829–3844.

Larson, A.C. and Von Dreele, R.B. (2000) General Structure Analysis System (GSAS). Los Alamos National Laboratory Report, LAUR 86-748.

Levien, L. and Papike, J.J. (1976) Scapolite crystal chemistry: Aluminum-silicon distributions, carbonate group disorder, and thermal expansion. American Mineralogist, 61, 864–877.

Lin, S.B. and Burley, B.J. (1973) On the weak reflections violating body-centered symmetry in scapolites. Tschermaks Mineralogische-Petrologische Mitteilungen, 20, 28–44.

Lovering, J.F. and White, A.J.R. (1969) Granulitic and eclogitic inclusions from basic pipes at Delegate, Australia. Contributions to Mineralogy and Petrology, 21, 9–52.

Moecher, D.P. and Essene, E.J. (1990) Phase-equilibria for calcic scapolite, and implications of variable Al-Si disorder for *P-T*, T-X_{CO_2}, and a-X relations. Journal of Petrology, 31, 997–1024.

——— (1991) Calculation of CO_2 activities using scapolite equilibria: Constraints on the presence and composition of a fluid phase during high-grade metamorphism. Contributions to Mineralogy and Petrology, 108, 219–240.

Seto, Y., Shimobayashi, N., Miyake, A., and Kitamura, M. (2004) Composition and $I4/m$-$P4_2/n$ phase transition in scapolite solid solutions. American Mineralogist, 89, 257–265.

Shaw, D.M. (1960) The geochemistry of scapolite. Part I. Previous work and general mineralogy. Journal of Petrology, 1, 218–260.

Sherriff, B.L., Sokolova, E.V., Kabalov, Y.K., Teertstra, D., Kunath-Fandrei, G., Goetz, S., and Jäger, C. (1998) Intermediate scapolite: ^{29}Si MAS and ^{27}Al SATRAS NMR spectroscopy and Rietveld structure-refinement. Canadian Mineralogist, 36, 1267–1283.

Sherriff, B.L., Sokolova, E.V., Kabalov, Y.K., Jenkins, D.M., Kunath-Fandrei, G., Goetz, S., Jäger, C., and Schneider, J. (2000) Meionite: Rietveld structure-refinement, ^{29}Si MAS and ^{27}Al SATRAS NMR spectroscopy, and comments on the marialite-meionite series. Canadian Mineralogist, 38, 1201–1213.

Sokolova, E.V., Kabalov, Y.K., Sherriff, B.L., Teertstra, D.K., Jenkins, D.M., Kunath-Fandrei, G., Goetz, S., and Jäger, C. (1996) Marialite: Rietveld structure-refinement and ^{29}Si MAS and ^{27}Al satellite transition NMR spectroscopy. Canadian Mineralogist, 34, 1039–1050.

Sokolova, E.V., Gobechiya, E.R., Zolotarev, A.A., and Kabalov, Y.K. (2000) Refinement of the crystal structures of two marialites from the Kukurt deposit of the east Pamirs. Crystallography Reports, 45, 934–938.

Teertstra, D.K. and Sherriff, B.L. (1996) Scapolite cell-parameter trends along the solid-solution series. American Mineralogist, 81, 169–180.

Teertstra, D.K., Schindler, M., Sherriff, B.L., and Hawthorne, F.C. (1999) Silvialite, a new sulfate-dominant member of the scapolite group with an Al-Si composition near the $I4/m$-$P4_2/n$ phase transition. Mineralogical Magazine, 63, 321–329.

Toby, B.H. (2001) EXPGUI, a graphical user interface for GSAS. Journal of Applied Crystallography, 34, 210–221.

Ulbrich, H.H. (1973) Structural refinement of the Monte Somma scapolite, a 93% meionite. Schweizerische Mineralogische und Petrographische Mitteilungen, 53, 385–393.

MANUSCRIPT RECEIVED SEPTEMBER 12, 2007
MANUSCRIPT ACCEPTED MARCH 4, 2008
MANUSCRIPT HANDLED BY LAURENCE GALOISY